

FSU-SCRI-94-71
HU Berlin-IEP-94/10
July 15, 1994

SCALING IN THE POSITIVE PLAQUETTE MODEL AND UNIVERSALITY IN SU(2) LATTICE GAUGE THEORY

J. Fingberg,^a U.M. Heller^a and V. Mitrjushkin^b

^a SCRI, Florida State University, Tallahassee, FL 32306-4052, USA.

^b Institut für Physik, Humboldt-Universität zu Berlin, 10099 Berlin, Germany. ¹

Abstract

We investigate universality, scaling, the β -function and the topological charge in the positive plaquette model for SU(2) lattice gauge theory. Comparing physical quantities, like the critical temperature, the string tension, glueball masses, and their ratios, we explore the effect of a complete suppression of a certain lattice artifact, namely the negative plaquettes, for SU(2) lattice gauge theory. Our result is that this modification does not change the continuum limit, *i.e.*, the universality class. The positive plaquette model and the standard Wilson formulation describe the same physical situation. The approach to the continuum limit given by the β -function in terms of the bare lattice coupling, however, is rather different: the β -function of the positive plaquette model does not show a “dip” like the model with standard Wilson action.

¹Permanent address: Joint Institute for Nuclear Research, Dubna, Russia

1 Introduction

The pure gauge sector of lattice QCD, though at present the most studied part of the theory in numerical simulations, still provides many open questions. One of the most interesting yet unresolved problems is connected with the mechanism of confinement at low temperatures. Among the possible solutions to this problem one could mention the dual superconductivity mechanism [1] or the effective Z_2 theory of confinement [2] based on a Z_2 -vortex condensation mechanism [3]. However, as is well-known, the lattice formulation of any quantum field theory is not unique. Different lattice theories, equivalent on a classical level, may possess completely different phase structures. As a result these models can have different continuum limits, *i.e.*, belong to different universality classes (for a recent example see [4]). In order to get reliable “physical” results for continuum physics from numerical calculations, it is therefore necessary to compare different forms of lattice actions.

The question of the choice of one or another lattice formulation can also be connected to the problem of lattice artifacts (for a short review see *e.g.* [5] and references therein). For example, small-scale ($\sim a$) fluctuations carrying a nontrivial topological charge can lead to the divergence of the topological susceptibility in the continuum limit (at least, for the geometric definition of the topological charge) [6, 7]. A source of trouble in this case are the special field configurations containing negative plaquettes, $\frac{1}{2}\text{Tr}U_P \sim -1$ (for $SU(2)$ gauge group). In more general form the question could be formulated as: how do *non-smooth* (rough) lattice field configurations influence the calculation of physical observables?

Another problem of general interest includes bad scaling behavior of $SU(N)$ gauge theories. Previous studies with the standard Wilson plaquette action (SWA) on lattices up to $48^3 \times 16$ at finite temperature [8] and up to $48^3 \times 56$ at zero temperature [9] showed that (asymptotic) scaling violating terms are still strong at the β -values accessible to today's numerical simulations. These terms manifest themselves most strikingly in the famous dip of the “step β -function”, $\Delta\beta(\beta)$. This pattern is similar in all $SU(N)$ gauge theories with a wide set of different actions.

A lot of promising attempts to overcome these difficulties are based on the use of “improved” actions and/or effective coupling schemes. The latter, of course, only affect the asymptotic scaling behavior, now in terms of the effective, instead of the bare, coupling. Improved actions, on the other hand, should diminish scaling violations and improve the control over dislocations. At the same time they should be in the same universality class as

the standard Wilson action, and hence lead to the same continuum limit.

This work is devoted to the study of the long-distance properties in the theory with a modified action where negative plaquettes are suppressed (positive plaquette model). Previous investigations of the positive plaquette model (PPM), first considered by Mack and Pietarinen [10] and Borneyakov, Creutz and Mitrjushkin [5] (see also [11]), suggest that large-scale objects, e.g. Polyakov loop correlators, Wilson loops and Creutz ratios, are strongly influenced by lattice artifacts even at comparatively large values of the inverse coupling β . The size-dependence of Wilson loops was shown to be consistent with an area law but the scaling properties of the string tension, *i.e.*, the fate of confinement in this model, were left beyond the scope of both papers [10, 5].

The dip in the “step β -function”, $\Delta\beta(\beta)$, observed for the standard model might be associated with the presence of negative plaquettes, definite lattice artifacts which vanish in the continuum limit. This dip has been associated with the phase structure when adding an adjoint coupling, insensitive to the sign of $\text{Tr}U_p$, to the standard fundamental one. The phase structure stems from the fact that as $\beta_a \rightarrow \infty$ the plaquettes are frozen to ± 1 [12], but in the PPM the value -1 is not allowed and therefore the phase transition at large β_a , whose critical endpoint close to the fundamental axis is supposed to be responsible for the dip, does not occur. The interesting question then is, whether the removal of negative plaquettes really avoids this dip and whether it improves the approach to the continuum limit.

A possible verification of this scenario requires a test of universality and a comparison of the scaling and asymptotic scaling behavior in the PPM and the conventional SU(2) lattice gauge theory. This task has been accomplished by a comprehensive study of the PPM both at finite and zero temperature. Our strategy consisted of two steps. First we determined the critical couplings for various lattice sizes and measured some universal quantities. These results were then used in an investigation of the model at vanishing temperature which consisted of a measurement of the heavy quark potential and the glueball spectrum of the two lowest excitations. We found it important to study a wide set of mass ratios in order to test whether some of these operators are influenced more strongly than others. Our work was completed by an MCRG analysis of the step β -function and a measurement of the topological charge and susceptibility. It should be noted that the removal of negative plaquettes is an entirely non-perturbative modification of the Wilson action. The perturbation theory remains unchanged. In particular, the Λ -parameter remains unchanged, as does the inverse coupling in the continuum limit, *i.e.*, $\beta_{PPM} = \beta_W$ as $\beta_W \rightarrow \infty$.

For the present study we have chosen a complete suppression of negative plaquettes, *i.e.*, a cutoff for the plaquettes at zero. Any other value smaller than 1 would have been possible for this cutoff. However, as we will see, the critical coupling β_c for the deconfinement transition in the PPM for $N_\tau = 2$ is already very small. Therefore, for choices of the cutoff larger than zero, lattices with a small extent in the time direction might no longer be confined at positive values of the gauge coupling. While this does not have to affect the continuum limit, it makes a numerical investigation far more difficult, since much larger lattices would need to be considered.

In the following section we describe the details of our simulations. Then we discuss our results obtained at finite temperature. In sections 4 and 5 we present our results for the heavy quark potential and the glueball spectrum. The next section is dedicated to a detailed MCRG analysis of the step β -function. In section 7 we combine these findings and discuss their implication for scaling and asymptotic scaling. Finally we summarize our results and come to the conclusions.

2 The simulations

In this work the calculations were done on symmetric lattices with size up to 16^4 and on asymmetric ones with temporal extent $N_\tau = 2, 4$ and 8 and spatial extent up to $N_\sigma = 24$. The values of the gauge coupling β we used covered the interval between zero and 2.6.

For most of the simulations, whose results will be described in the subsequent sections, we have used a mixture of 4 microcanonical overrelaxation sweeps followed by one heat bath sweep. In the microcanonical step

$$U_l \rightarrow U'_l = W^\dagger U_l^\dagger W^\dagger \quad (1)$$

where W is the “staple” projected onto the $SU(2)$ group, one or more of the 6 plaquettes which contain the link l can become negative. If this occurs, the change is, of course, rejected. This rejection rate, quite large at small β , fortunately decreases rapidly with increasing β where the autocorrelation time becomes larger and the overrelaxation steps therefore more important.

The heat bath updating was done for smaller β using the Creutz algorithm [13] and for larger β the Kennedy–Pendleton version [14]. The choice of version was done by measuring the CPU time of short trial runs. In both heat bath versions we added, of course, rejection of trial link updates that produce negative plaquettes to the usual criterion.

In the runs at very small β 's the heat bath acceptance rate dropped dramatically due to the frequency of proposed links that give negative plaquettes and have to be rejected. There we used, instead, a Metropolis algorithm with the size of the proposed random changes tuned to give an acceptance rate of about 50%.

We performed simulations on asymmetric lattices with $N_\tau = 2, 4$ and 8 to study the deconfinement transition. In those simulations we measured the Polyakov line after every heat bath (Metropolis) sweep. In the simulations on symmetric lattices, used for the MCRG study and the measurement of the string tension, glueball masses and topological susceptibility, we typically measured after every 20 heat bath sweeps. In this way, about the same amount of CPU time was spent on updating and on all the measurements. It also turned out that this spacing — recall that 4 overrelaxation sweeps were done before every heat bath sweep — made the measurements essentially independent, with integrated autocorrelation length $\tau_{auto} \lesssim 1$.

3 The deconfinement temperature

To check the universality of continuum physics obtained with the PPM and the theory with the SWA, one should compare results obtained in “equal physical circumstances”. In particular the lattice coupling must be chosen carefully. The easiest way to do this is to study the deconfinement transition on lattices with the same temporal extent N_τ . This will ensure that we compare the two theories at equal lattice spacings. Later on we will determine other physical (zero-temperature) observables, like the string tension and glueball masses, at the critical couplings. This will allow us a direct comparison of ratios like $T_c/\sqrt{\sigma}$ at equal lattice spacings in physical units.

The PPM, like the $SU(2)$ theory with SWA, has a global Z_2 symmetry, which gets spontaneously broken when the system crosses the critical temperature. The transition is therefore expected to be of second order, in the universality class of the 3 dimensional Ising model. However some care is necessary, since universality may get disrupted by a change of the action and therefore should be submitted to tests. (It is worthwhile to note that there is no finite temperature phase transition at $N_\tau = 1$ at least at positive β 's [5]).

Finite-size scaling (FSS) techniques have proven to be effective tools to explore the critical properties of statistical systems [15]. In combination with the density of states method a comprehensive study of the region of the deconfinement transition becomes possible. We

investigated the PPM at finite temperature by measuring the order parameter, which is the expectation value of the Polyakov loop, $\langle |L| \rangle$, its susceptibility χ and its 4th-order (Binder) cumulant, g_4 , [16] in order to determine critical couplings and test universality by a consistency check of critical exponents. A completely independent determination of the critical exponents would have been beyond the scope of this paper.

We investigated the phase transition for systems with temporal extent $N_\tau = 2, 4$ and 8. The most extensive study was done for $N_\tau = 4$, where we used three different spatial lattice sizes, while for the others we only considered two. The parameter values for our finite temperature runs as well as the results for the Polyakov loop expectation values are summarized in Tab. 1. We determined the critical couplings from the crossing of curves of g_4 versus β belonging to different N_σ at fixed N_τ . The result is shown in Fig. 1. The values we extracted for the critical couplings are listed in Tab. 2. A comparison with results for the SWA shows a huge shift in the critical coupling, when compared at fixed value of $N_\tau = 2, 4$ and 8. This large shift at strong coupling should be contrasted to the fact that in the continuum limit, *i.e.*, for very large N_τ , the critical couplings should become identical. Thus we can already conclude that the “step β -functions” for the PPM and with SWA will be quite different.

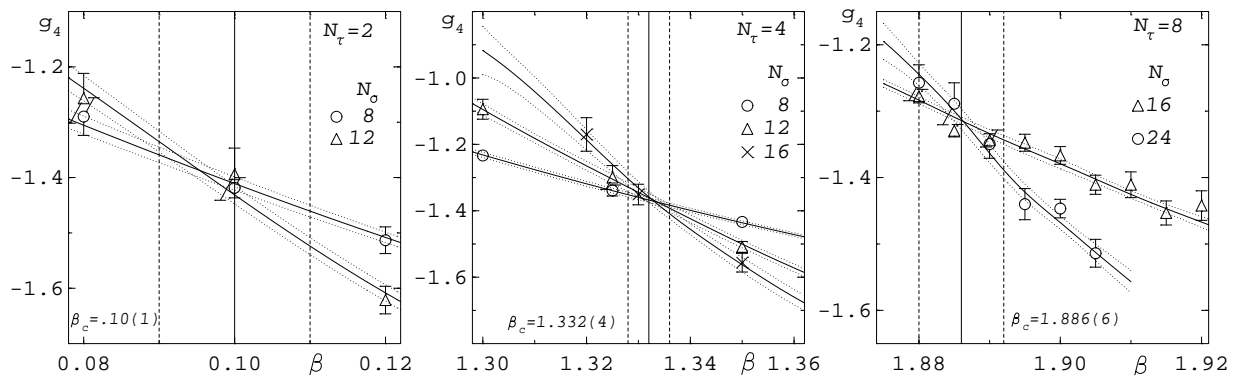


Figure 1: The 4th order cumulant g_4 for $N_\tau=2, 4$ and 8. The continuous curves together with their error bands were obtained by standard reweighting.

The value of the cumulant g_4 at the critical couplings is expected to be a universal quantity. In all cases, $N_\tau = 2, 4$ and 8, it is in good agreement with the value $g_4 = -1.38(5)$, which was found for the SWA [18]. We find that the Binder cumulant g_4 shows the same

FSS behavior for the PPM, that already has been verified for the SWA [18, 8]. The low temperature phase susceptibility χ_v is expected [17, 19] to behave like

$$\chi_v = N_\sigma^d \langle L^2 \rangle = (N_\sigma/N_\tau)^{\frac{\gamma}{\nu}} Q_{\chi_v}(g_4; N_\tau) \quad (2)$$

A FSS test [19] for $N_\tau = 4$, where we have 3 different lattice sizes, based on Eq. (2) consists of plotting the scaling function $\tilde{Q}_{\chi_v} = N_\sigma^{d-\frac{\gamma}{\nu}} \langle L^2 \rangle$ as a function of g_4 . Inserting the value $\gamma/\nu = 1.970(11)$ of the 3-dimensional Ising model [20] this test has the advantage that there are no free parameters left. The result is shown in Fig. 2. We expect that data points coming from different volumes fall on a unique curve, if finite-size scaling with the Ising value of the ratio γ/ν holds. Our data points shown in Fig. 2 agree very well with this assumption.

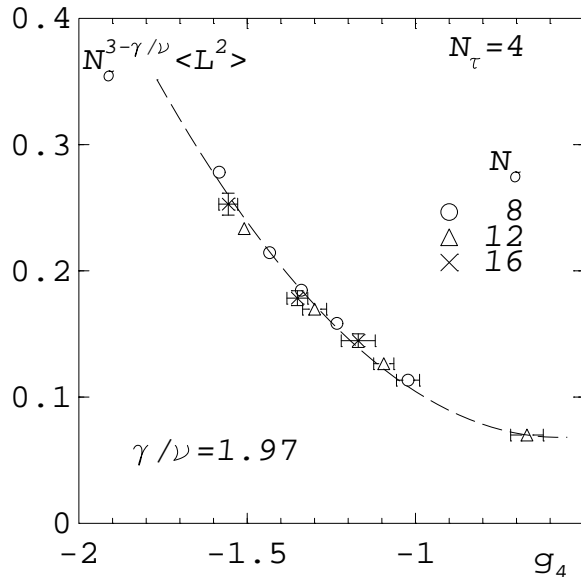


Figure 2: Finite-size scaling of the susceptibility. The curve is a parabola drawn to guide the eye.

Therefore, we conclude that the finite temperature phase transition in the PPM with $SU(2)$ gauge symmetry belongs to the same universality class as the phase transition in the $3d$ Ising model, and the finite temperature phase transition in the standard Wilson theory.

4 Heavy quark potential

We are interested in comparing some physical observables obtained in the PPM to those obtained with the SWA. Such a comparison will tell us whether the continuum limit of the two models is the same, as suggested by universality. To allow a direct comparison we chose equal lattice spacings (in physical units) by performing (some of) the simulations at the critical couplings of the deconfinement transition on lattices with the same temporal extent N_τ for both actions.

For such a comparison we chose the heavy quark potential, from which one can extract the string tension. With the recently developed signal improving techniques [21] the heavy quark potential can be measured quite accurately without the need for very large statistical samples. The signal improvement consists in replacing the links that make up the space-like segments of (time-like) Wilson loops with recursively constructed “smeared” links. Besides planar Wilson loops, with on-axis space-like segments, we also considered Wilson loops with off-axis space-like segments along the paths (1,1,0) and (2,1,0) and those related by the cubic symmetry.

Smearing of the space-like links gives a better overlap with the lowest state in the exponential behavior

$$W(\vec{R}, T) = \sum_i c_i(\vec{R}) \exp\{-V_i(\vec{R}) \cdot T\} \quad (3)$$

with $V(\vec{R}) = V_0(\vec{R})$ the heavy quark potential we would like to find. With a better overlap the effective potential, extracted from

$$V_T(\vec{R}) = \log \left(\frac{W(\vec{R}, T)}{W(\vec{R}, T+1)} \right) \xrightarrow{T \rightarrow \infty} V(\vec{R}) \quad (4)$$

will have an earlier plateau in T , where the statistical errors are still small.

We fit the potential, taken as the effective potential at a given T , to the usual form [22]

$$V(\vec{R}) = V_0 + \sigma R - \frac{e}{R} - f \left(G_L(\vec{R}) - \frac{1}{R} \right) \quad . \quad (5)$$

Here G_L denotes the lattice Coulomb potential, which takes into account the lattice artifacts present at smaller distances; it helps in getting good fits that also include rather small distances. We used fully correlated fits with the covariance matrix estimated by a bootstrap method. In all cases, the best fit values obtained in this way did not differ significantly from those of naive, uncorrelated fits. To select one from the many possible fits, obtained when

varying the range over which the fit is performed, we define a “quality” of the fit as the product of confidence level times the number of degrees of freedom divided by the relative error of the string tension. We selected the fits with the highest quality and list the results in Table 3. The T in the third column gives the time separation from which the potential was determined as in eq. (4).

For the smallest β value considered, corresponding to the critical coupling of a finite temperature system with $N_\tau = 2$ (see the previous section), rotational invariance of the potential is quite strongly violated. Thus we made fits over the potential along a principle axis, and along the (1,1,0) directions separately and list the result in two rows of the Table 3. There was no sign of a Coulomb term — the string tension term completely dominates the potential — so we left it out from the fit.

For the next coupling, $\beta = 1.332$, the critical coupling of the $N_\tau = 4$ finite temperature transition, rotational invariance is already quite well restored. But, as an additional check we also fit over the on-axis potential and the potential along direction (1,1,0) separately and list them in rows 2 and 3 for each T .

To give an impression of the systematic uncertainty in the determination of the string tension we list in Table 3 the results for several T (see eq. (4)). For the largest coupling listed, $\beta = 2.2$, we see that even on the 16^4 lattice the fit parameters change rapidly with varying T . This indicates that the lattice is too small. Indeed, from the MCRG and T_c results we estimate that $\beta = 2.2$ is quite close to the critical coupling for the deconfinement transition with $N_\tau = 16$. We therefore regard the results for the coupling $\beta = 2.2$ as not trustworthy. Also for $\beta = 2.05$, even on the $L = 16$ lattice, we find no good convergence of the fit parameters to the potential. Thus, the string tension extracted for this coupling might still suffer from too small a lattice size. Keeping this in mind, we will nevertheless show results for $\beta = 2.05$.

For each coupling we chose the fit with the largest confidence level on the largest lattice in Table 3. The potentials with these fits, on the 16^4 lattices, are shown in Fig. 3. We show $a\sqrt{\sigma}$ versus the bare lattice coupling in Fig. 4, where for comparison we also included some values for the SWA. Since the bare couplings for equal lattice spacing in the PPM and SWA are rather different, the comparison becomes easier, if instead of the bare coupling, we use some effective coupling which is closer in both models. We chose the effective coupling β_E [23] for this (see also the Appendix). The comparison is shown in Fig. 4b, from which we see that now the behavior of the string tension looks very similar for both the PPM and

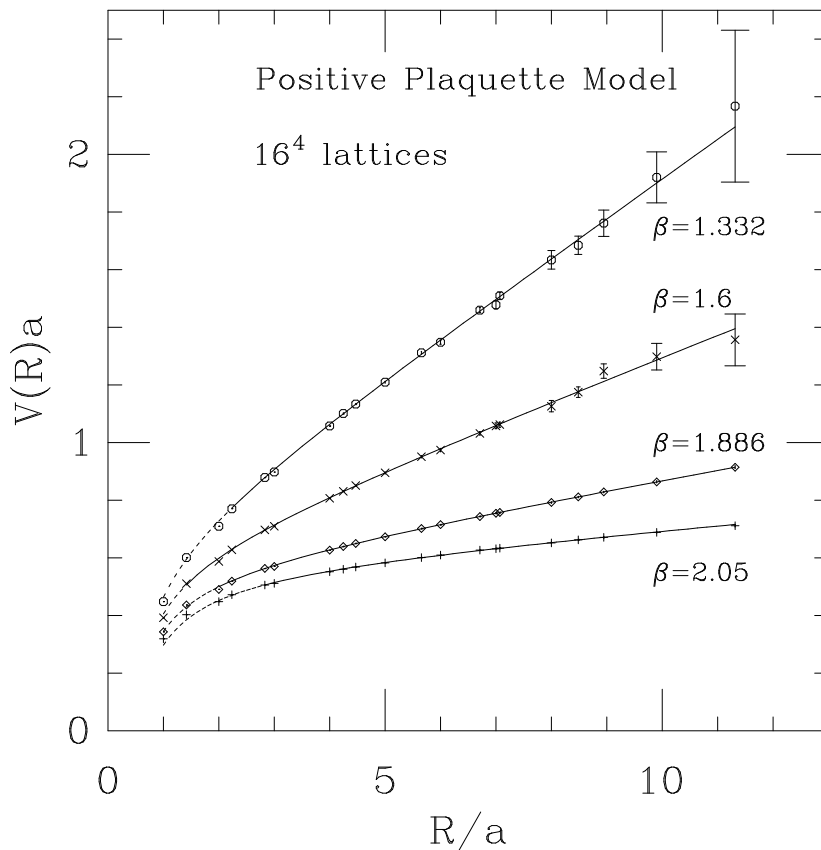


Figure 3: The heavy quark potential in the positive plaquette model from 16^4 lattices.

SWA once β_E becomes larger than a threshold in the region of ≈ 1.5 .

5 Glueball measurements

Other physical observables in pure glue gauge theories are the glueballs, in particular their masses. These mass measurements are notoriously difficult, especially for glueballs other than those with 0^{++} and 2^{++} quantum numbers. Since glueballs were not the focal point of our research, we restricted our measurement to the masses of glueballs with those two quantum numbers. They can be measured with simple plaquette correlation functions and thus we did not measure correlation functions between loops of bigger size and more complicated

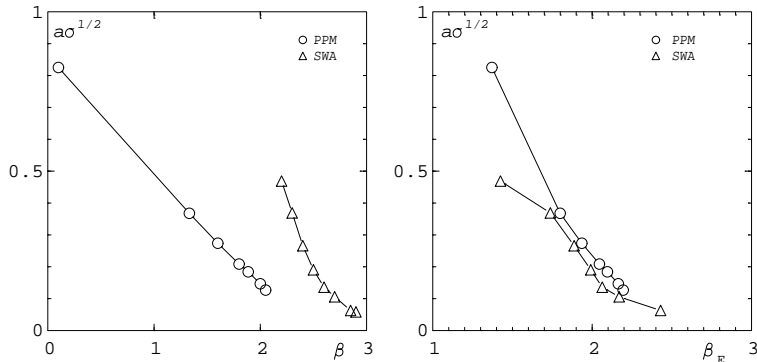


Figure 4: A comparison of the string tension in the PPM and for the SWA versus the bare lattice coupling (left) and the effective coupling β_E (right). We compare to SWA results from Refs. [38, 39, 40].

shape.

As for the measurement of the heavy quark potential some signal improvement technique is essential for the success of glueball measurements. Both smearing of links [21] and fuzzing [24] have been advocated before the “plaquettes” for the correlation functions are constructed. Since we already made smeared (space-like) links for the potential measurement we decided to try a hybrid of the two methods. We started with these smeared links and then applied fuzzing to them, measuring the plaquettes, summed over each time slice for zero-momentum projection, for each fuzzing level starting with the zeroth, the smeared links. In the analysis we could then construct the correlation functions at each fuzzing level as well as cross correlations between plaquettes at different fuzzing levels.

With P_{xy} being the (fuzzed) plaquette in the $x - y$ plane, etc., we considered the 0^{++} (cubic group A_1^{++}) glueball operator $P_{xy} + P_{xz} + P_{yz}$ and two 2^{++} (cubic group E^{++}) glueball operators, $P_{xz} - P_{yz}$ and $2P_{xy} - P_{xz} - P_{yz}$. We shall refer to these as tensor glueball I and II. In addition we measured the correlation function between Polyakov lines in the spatial directions, constructed from the fuzzed links. Their “mass” gives another measurement for the string tension, $m_{Pol} = L\sigma_{Pol}$, with L the spatial lattice size. In Fig. 5 we show the ratios of the correlation functions at distance a and 0. According to [25] this should give an indication of the optimal fuzzing level. Except for a somewhat mysterious dip at fuzzing level 2 for the scalar glueball, this ratio is almost independent of the fuzzing level. The

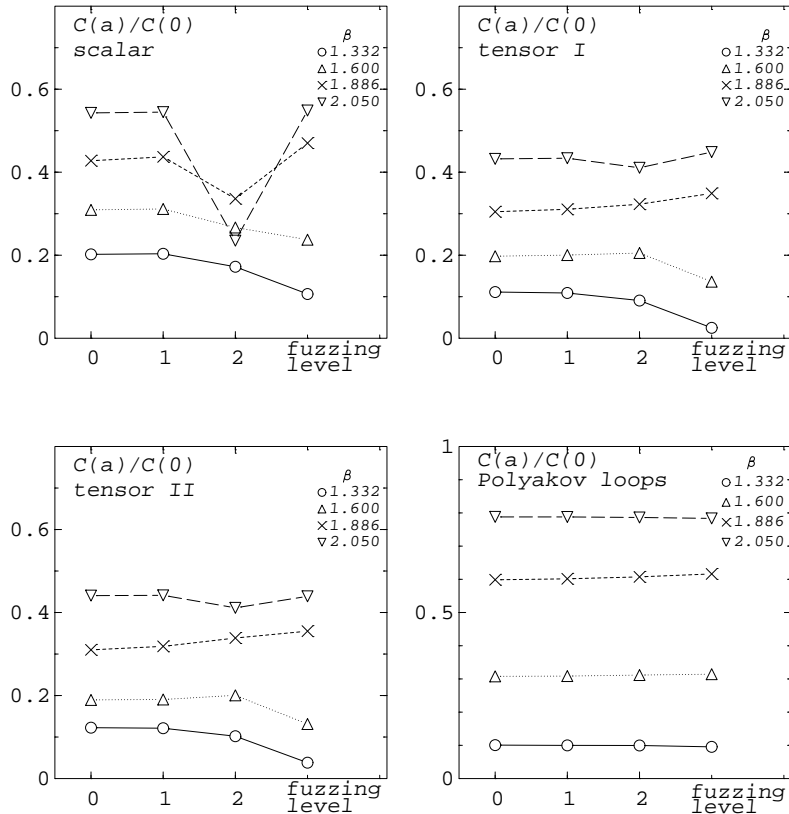


Figure 5: Normalized correlation functions for the scalar, the tensor I and II glueballs and Polyakov loops on 16^4 lattices.

reason is, that we started, at fuzzing level 0, with smeared links, which already give a good signal.

Since we measured all cross correlations between the operators with different fuzzing level, we tried the diagonalization procedure of [26] to improve the quality of the extracted masses. It did not make any improvement. It appears that the operators we used are too similar and hence couple almost equally to the various states in a channel with given quantum numbers. We therefore extracted the masses simply as effective, or running masses, from the correlation function at fuzzing level 1. The masses are listed in Table 4.

While masses have finite size effects that are exponentially suppressed with the system size, the string tension, as determined from Polyakov line correlations, has substantial finite size effects. They can be understood in terms of a picture of a fluctuating string [27]. The

fluctuations create a correction to the string tension, which depends on the lattice size, and drives $\sigma_{Pol}(L)$ to smaller values

$$a^2\sigma_{Pol}(L) = a^2\sigma_{Pol}(\infty) - \frac{\pi}{3N_\sigma^2}. \quad (6)$$

The finite size correction is 0.0073 for the 12^4 lattices and 0.0041 for the 16^4 lattices.

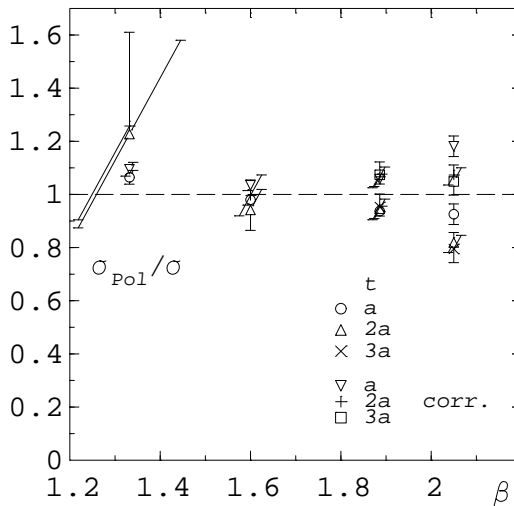


Figure 6: Ratio of the string tension from Polyakov lines, σ_{Pol} , and from fits to the heavy quark potential, σ . For σ_{Pol} we show both the finite volume values and the finite size corrected ones.

We have now two independent determinations of the string tension. We compare them in Fig. 6, where we show for σ_{Pol} both the directly measured finite volume values, as well as the values obtained with the finite size corrections of eq. (6). We see that the finite size corrections become quite substantial for the larger couplings, and make the agreement better. Of course, σ_{Pol} should be extracted from as large a t as possible, but generally the last two values agree.

6 MCRG results

With numerical methods one can not measure the β -function of a lattice field theory directly. But, employing Monte Carlo Renormalization Group (MCRG) methods, we can obtain the

“step β -function”, $\Delta\beta(\beta)$, for a given change of scale, in our case by a factor 2. This step β -function is the integrated β -function over the given finite change of scale.

We employed two different MCRG methods. The first is a real space RG with a blocking transformation proposed first by Swendsen [28] that has a parameter p which can be optimized to reach the renormalized trajectory after as few blocking steps as possible. The second is the so called “ratio method” in which appropriate ratios of Wilson loops, differing by a factor 2 in size, are matched. Following [29] we used, besides the “bare” ratios, tree-level and one-loop improved ratios in the matching procedure.

For the real space RG we used “blocking scheme 1” of [30], and followed the optimization procedure described in detail there. To narrow down the range of the optimization parameter p we made some trial runs comparing 8^4 with 4^4 lattices for each $\beta = \beta_L$ for which we wanted to find $\Delta\beta$. The optimal value of p is the one that gives the most consistent matching of all four observables that we used, the plaquette and the three different shaped loops of length 6, build from blocked links at the appropriate blocking level, after the fewest blocking steps. We used linear interpolation in $1/p$ as in Ref. [30]. Then we made runs with two values of p that appeared to bracket the optimal value, comparing 12^4 with 6^4 and 16^4 with 8^4 lattices. To be able to do the matching, we made two runs on the smaller lattices with slightly different couplings, β_S , and interpolated linearly between them. For each of the four observables we obtained in this way a $\Delta\beta = \beta_L - \beta_S$, with a statistical error determined by jackknife. We interpolated these to the optimal p values and then averaged them. The results are listed in Table 5. The errors quoted include the statistical errors, as well as systematic errors describing the spread of $\Delta\beta$ obtained from the different observables. The columns without the label “extr.” give the results of the matching of blocking level n on the larger lattice with blocking level $n - 1$ on the smaller lattice. The columns with the label “extr.” give the results after extrapolating from blocking levels n and $n - 1$ to an infinite number of blockings, taking into account only the leading irrelevant eigenoperator of the blocking RG transformation with eigenvalue $1/4$ [30],

$$\Delta\beta^{(\infty)} = \frac{1}{3} [4\Delta\beta^{(n)} - \Delta\beta^{(n-1)}]. \quad (7)$$

To implement the ratio method we measured planar Wilson loops with the variance reduced by the method of Parisi, Petronzio and Rapuano, [31]. Since, for the PPM we do not have a closed formula to compute the improved links, we calculated them with typically 20 hits. To increase the number of Wilson loops from which we can build ratios, especially

for the smaller lattices, we measured Wilson loops up to distances $L/2 + 2$. Since the finite size effects on the large and small lattices to be matched are the same this is acceptable for the ratio method. We would not advocate using Wilson loops larger than $L/2$ to extract, say, the potential.

Each Wilson loop ratio considered provides a $\Delta\beta$, again inferred from two β values on the smaller lattices by interpolation, with an error determined by jackknife. The results from “bare” ratios are afflicted by lattice artifacts, especially if the ratio contains small Wilson loops. These artifacts can be corrected for in perturbation theory by building appropriate linear combinations that give the correct result in perturbation theory at tree or one-loop level [29]. Since the perturbation expansion of the PPM and the theory with SWA are identical — the removal of negative plaquettes is a non-perturbative procedure — the perturbative Wilson loops of [32] can be used to construct the improved ratios.

Typically the improvement shows up in a smaller variance of the results from many different ratios. The results listed in Table 6 represent the average $\Delta\beta$ over all ratios satisfying certain “cuts” [29]. The cuts, given in sizes appropriate for the smaller of the two lattices matched, are (i) maximal length R_{max} of the sides of a Wilson loop (since we measured loops up to size $L/2 + 2$) (ii) the minimal area A_{min} of Wilson loops included (to cut off small distance lattice artefacts), (iii) area difference ΔA_{min} in numerator and denominator of a ratio (the larger this difference is, the faster the ratio varies with the coupling and the easier it is to find a good matching) and (iv) maximal statistical error δ_{max} in $\Delta\beta$ from a ratio. The errors quoted in Table 6 are the variances over the ratios that passed all cuts.

Our results for $\Delta\beta$ from the determination of T_c and from the MCRG analysis are shown in Fig. 7. We see that the dip produced by the SWA is completely removed. The function is monotonous in the whole range accessible to our simulations. It comes down steeply from above at small β values and converges rather slowly to the perturbative limit. A comparison at fixed N_τ , i.e., equal lattice spacing, indicates that the convergence in the PPM is even slower than with the SWA. It should be noted that, since the perturbative β -functions in the PPM and with SWA are identical, the approach of $\Delta\beta(\beta)$ to the 2-loop form eventually, for very large β , has to be the same. Depending on the sign of the order $1/\beta$ contribution, which contains the 3-loop coefficient of the β -function, it comes from above or below. Thus for either the PPM or the SWA $\Delta\beta(\beta)$ has to cross the 2-loop curve and have another small “dip” or “hill”.

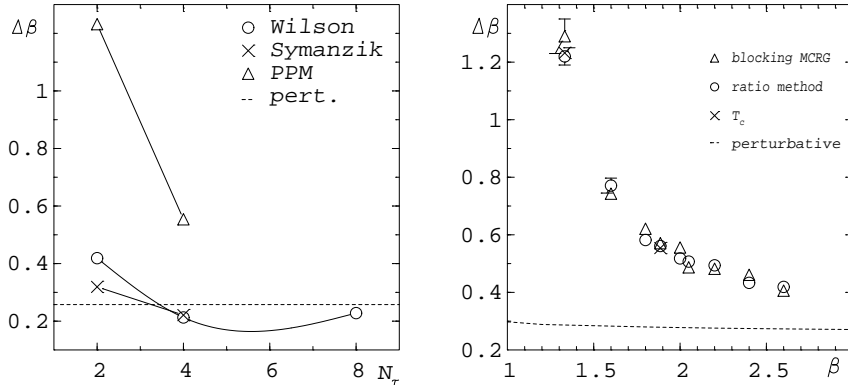


Figure 7: The discrete β -function from measurements of T_c and from an MCRG analysis. The figure on the left shows a comparison of the SWA and the PPM as well as a Symanzik improved action [33]. In the figure on the right we compare the “step β -function” $\Delta\beta$ obtained by various methods. Data from the largest lattice and/or highest blocking level were used.

7 Scaling and asymptotic scaling

The results of the last section tell us, that, in the range of couplings accessible to numerical simulations with moderate resources, we are still rather far from asymptotic scaling, especially as a function of the bare lattice coupling. This can be seen in Table 7 and Fig. 8 where we show the critical temperature converted to units of $\Lambda_{\overline{\text{MS}}}$ using the perturbative 2-loop relation. Besides giving the values for the bare lattice coupling we also considered an effective coupling scheme β_E [23] (see also the Appendix).

As expected from MCRG results, we see that the approach to asymptotic scaling for the PPM, in contrast to the SWA, is monotonous. The convergence rate seems comparable in both models. As for the SWA we find that using the effective coupling scheme, β_E , improves the asymptotic scaling behavior considerably. This shows that it takes into account non-perturbative effects beyond the level of negative plaquettes. Similar behavior is found for string tension and 0^{++} glueball mass, as shown in Fig. 9.

While the investigation of the asymptotic scaling behavior is important to make the connection with weak coupling perturbation theory, it is the “scaling” behavior that is important to determine the continuum limit. As usual we denote as “scaling” when dimensionless ra-

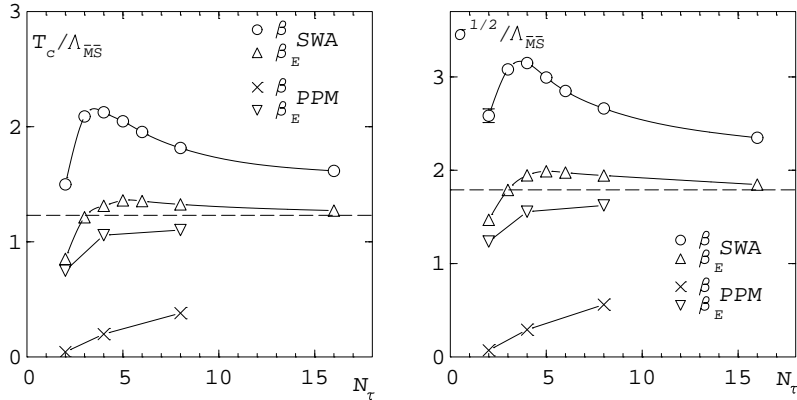


Figure 8: Asymptotic scaling of the critical temperature and the string tension from fits of the heavy quark potential with the bare (β) and an effective coupling (β_E). The dashed lines indicate the continuum values as determined in Ref. [8].

tios of physical quantities become independent of the bare coupling — or equivalently the lattice spacing a . Having, among other physical observables, measured the deconfinement transition temperature $T_c = 1/(a(\beta_c(N_\tau))N_\tau)$ and the string tension, we can test for scaling of the ratio $\sqrt{\sigma}/T_c = \sqrt{\sigma} a(\beta_c(N_\tau))N_\tau$. This is listed in Table 8 and shown in Fig. 10. As for the standard SU(2) lattice gauge theory, scaling is well obeyed between the critical couplings for $N_\tau = 4$ and 8. In addition, within errors the ratio $\sqrt{\sigma}/T_c$ in the PPM is the same as for the SWA, $\sqrt{\sigma}/T_c = 1.45(4)$ [8]. This shows that the two lattice models will have the same continuum limit.

We can test for scaling using other ratios: Fig. 11 shows the ratio of the tensor and the scalar glueball mass. Scaling is seen, within errors, for $\beta > 1.3$. Comparing with results from the SWA by Michael and Teper [25] we see that the PPM value is lower when the glueball masses are extracted from $t = a$ but are fully consistent with the continuum result $m(2^{++})/m(0^{++}) = 1.45(7)$ from Ref. [34] when extracted from $t = 2a$. The PPM value for the ratio $m(0^{++})/\sqrt{\sigma}$, shown in Fig. 12, again shows scaling and looks consistent with the result for the SWA by Michael and Teper of $3.87(12)$, as quoted in [34].

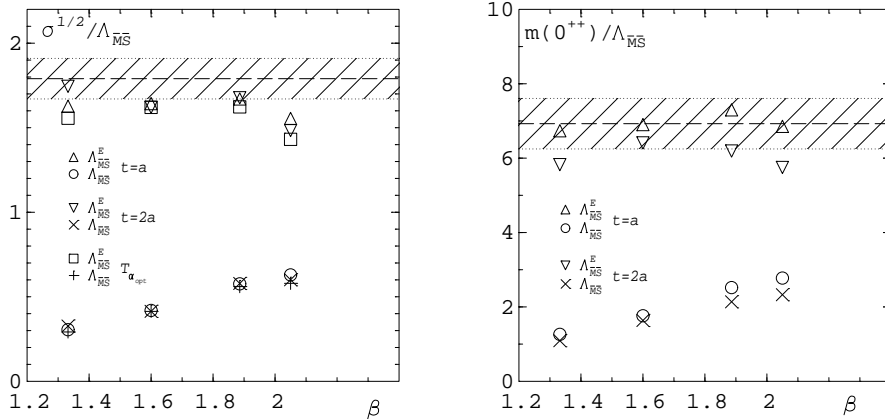


Figure 9: Asymptotic scaling of the string tension determined from the potential and Polyakov loops (with finite-size correction) and the scalar glueball mass. In the left figure the hatched region shows the continuum value $\sqrt{\sigma}/\Lambda_{\overline{\text{MS}}} = 1.79(12)$ determined in Ref. [8]. In addition the corresponding region in the figure on the right is based on the continuum value $m(0^{++})/\sqrt{\sigma} = 3.87(12)$ from Ref. [34].

8 Topology

An important (global) property of a gauge field configuration in the continuum is its integer valued topological charge. On the lattice the unique assignment of an integer valued topological charge is hampered by lattice artifacts. Indeed, for an $SU(2)$ lattice gauge theory short distance fluctuations on the size scale of one lattice spacing, so called dislocations, are believed to dominate the topological charge and the corresponding susceptibility on ensembles of configurations produced in a numerical simulation [6, 7].

The occurrence of negative plaquettes in configurations distributed according the SWA is a short distance lattice artifact. The suppression of negative plaquettes might also suppress (some of) the dislocations afflicting the topological susceptibility measurements. To check this we have measured the topological charge and susceptibility in our numerical simulations of the PPM.

The dislocations manifest themselves for example by the fact that even the geometric Philipps–Stone algorithm [35], can not assign a unique topological charge to a given gauge field configuration. Indeed, there are 8 ways to cut hypercubes into simplices using the differently oriented hypercube body–diagonals, and with this 8 different measurements of the topological charge. Were the charge assignment unique all 8 calculations would give the

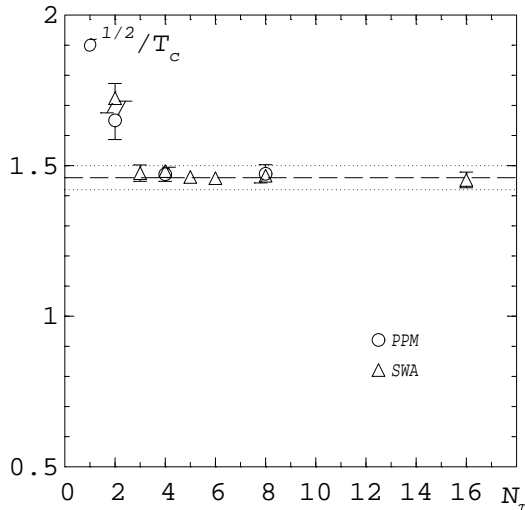


Figure 10: Scaling of the ratio of the square root of the string tension and the critical temperature. The dashed line indicates the continuum value as determined in Ref. [8].

same result. Due to the presence of dislocations this is not the case. To get a measure of the non-uniqueness we computed the average covariance

$$CV_{PS} = \frac{1}{28} \sum_{1 \leq i < j \leq 8} \frac{\langle (Q_i - \langle Q_i \rangle) (Q_j - \langle Q_j \rangle) \rangle}{\sqrt{\langle (Q_i - \langle Q_i \rangle)^2 \rangle \langle (Q_j - \langle Q_j \rangle)^2 \rangle}} \quad (8)$$

between the 8 different measurements — we used an implementation of the Philipps–Stone algorithm [36] generously provided to us by Micheal Müller-Preussker — on 6^4 and 8^4 lattices at the critical coupling for the $N_\tau = 4$ deconfinement transition. We found 0.404(15) and 0.397(13) for the SWA and 0.519(16) and 0.531(15) for the PPM, whereas a unique charge assignment would give unity. This shows that while the PPM, at equal lattice spacing, does somewhat better than the SWA, it still contains dislocations.

Since some dislocations are still present we used the cooling method [37] to eliminate the short distance fluctuations. Already after 5 cooling sweeps the average covariance, CV_{PS} , between the 8 different measurements was bigger than 0.99.

The geometric Philipps–Stone algorithm is very time consuming. Therefore we measured, on cooled configurations, also the naive, non-integer topological charge with a “clover” definition for $F_{\mu\nu}$ on the lattice. Already after 5 cooling sweeps the covariance between

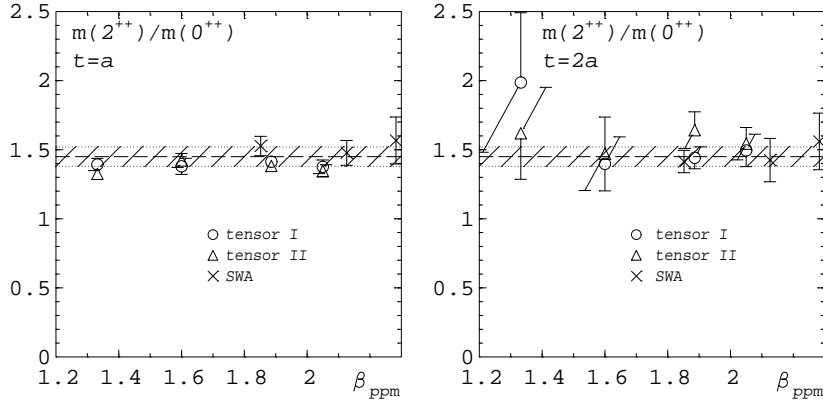


Figure 11: Scaling of the ratio of the tensor and the scalar glueball mass. The hatched region indicates the continuum value for the SWA from Ref. [34]. Results at $\beta_{SWA}=2.5, 2.7$ and 2.9 are from [38]. The conversion from β_{SWA} to β_{PPM} was done by matching the string tension from the heavy quark potential.

naive and geometrical topological charge definitions was about 0.96 for both PPM and SWA, and slowly increasing with further cooling sweeps. By rounding the non-integer charge, if the absolute value is bigger than 0.1, to the nearest integer away from zero (“ceiling” of the absolute value) we can assign an integer charge to each configuration. This procedure decreases the covariance to the geometrical charge slightly: after 5 cooling sweeps it is now about 0.91. However, out of the few variants that we tried to assign an integer charge from the naive non-integer charge, this version gave the best agreement of the susceptibility with that from the geometrical charge, after 5 (and more) cooling sweeps.

In the production runs for all the other measurements, described earlier, we measured the naive topological charge on cooled lattices, after 10, 15 and 20 cooling sweeps. We computed the topological susceptibility both with the non-integer charge and the integer charge obtained from it by rounding away from zero. They are listed in Table 9. For the 8^4 and 12^4 configurations we also used the geometric Philipps–Stone algorithm for the topological charge measurement. We did these measurements on the “hot” configurations, and after 15 coolings sweeps. The latter helps in estimating the systematic uncertainties that result from use of a naive definition of the topological charge, even on cooled configurations. The large drop of the susceptibility between hot and cooled configurations indicates that on hot configurations it is dominated by short distance dislocations, even in the PPM.

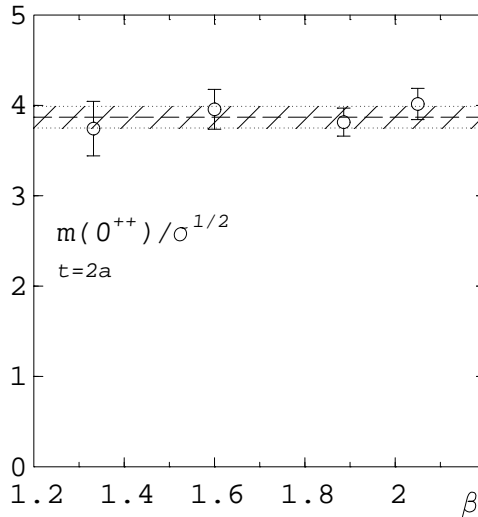


Figure 12: Scaling of the ratio of the scalar glueball mass and the square root of the string tension. The hatched region corresponds to the continuum value $m(0^{++})/\sqrt{\sigma} = 3.87(12)$ from Ref. [34].

Fig. 13 shows that the dimensionless ratio $R_t = \chi_t^{1/4}/\sqrt{\sigma}$ is a smooth function of the lattice spacing consistent with a continuum limit $R_t \approx 0.5$. We used the naive charge rounded away from zero (N2) after 15 cooling steps on the 16^4 lattices. This definition gave consistent results with its counterpart on the 12^4 lattices and the topological charge measured with the geometric Philipps–Stone algorithm.

A comparison with results from Ref. [38] shows that the results for the PPM and those obtained with the SWA agree very well. Only the PPM value of R_t at the largest coupling $\beta = 2.05$, corresponding to the smallest $a\sqrt{\sigma}$, seems to be too high. The reason for this is again that the lattice size, $L = 16$, might be too small.

9 Conclusion

We made a comprehensive study of scaling properties at zero and finite temperatures in the pure gauge $SU(2)$ theory with negative plaquettes suppressed (PPM), aimed at the comparison with the corresponding properties in the standard Wilson theory. This study included the calculation of the heavy quark potential, the masses of 0^{++} and 2^{++} glueballs, the “step

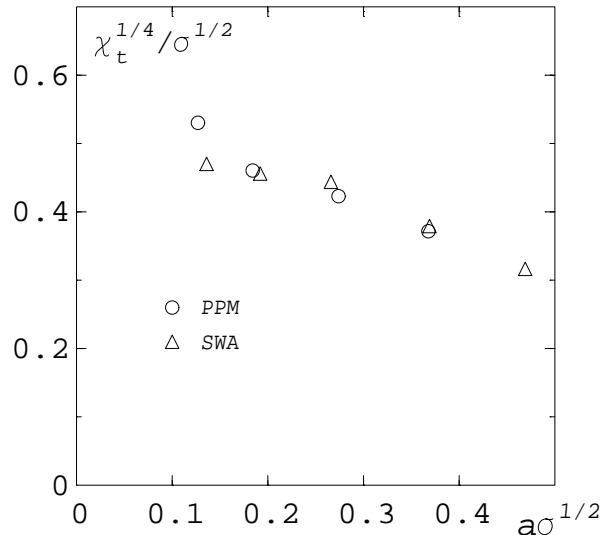


Figure 13: Scaling test of the ratio of the topological susceptibility (15c,N2) and the square root of the string tension as a function of $a\sqrt{\sigma}$. Results for the SWA were obtained by Michael and Teper in Ref. [38].

β -function”, $\Delta\beta(\beta)$, and the topological charge with its susceptibility. To monitor the finite temperature phase transition we calculated the Polyakov loops with their susceptibility and Binder cumulant. The calculations were done on symmetric lattices with size up to 16^4 and on asymmetric ones with temporal extent $N_\tau = 2, 4$ and 8 . The values of the gauge coupling β we used covered the interval between zero and 2.6 .

Our main conclusion is that the PPM belongs to the same universality class as the standard Wilson theory. For $\beta < \beta^*(L)$, where $\beta^*(16) \sim 2.05$, the heavy quark potential, $V(R)$, exhibits the linearly rising, confining behavior at large enough R . The physical ratios $m(2^{++}) : m(0^{++}) : \sqrt{\sigma} : \chi_t^{1/4}$ (the latter computed after cooling) show similar scaling patterns in the PPM and the conventional formulation.

In the finite temperature sector of the PPM we find a clear signal for a 2nd order phase transition with critical exponents consistent with the 3-dimensional Ising values. This shows that the PPM modification to the SWA maintains the universality class, a necessary condition to assure that the PPM and the theory with SWA describe the same physics in the continuum limit.

However, the approach to the asymptotic scaling behavior changed drastically after the suppression of one type of lattice artifacts, namely the occurrence of negative plaquettes in the gauge field configurations. In contrast to the SWA case the dependence of $T_c/\Lambda_{\overline{\text{MS}}}$ and $\sqrt{\sigma}/\Lambda_{\overline{\text{MS}}}$ on the lattice coupling or, equivalently, the lattice spacing is monotonous. Furthermore the dip of the SWA step β -function is completely removed. The PPM step β -function comes steeply from above and converges rather slowly to the perturbative 2-loop value. This shows that phenomena connected to the occurrence of negative plaquettes are the origin of this structure. The effective coupling scheme derived from the plaquette expectation value improves asymptotic scaling equally well for the PPM and the SWA.

As was expected, for the computation of the topological charge with the geometric Philipps–Stone algorithm on “hot” configurations, the modified action does somewhat better, compared to the Wilson action, because the configurations are somewhat smoother. Nevertheless, the suppression of negative plaquettes does not resolve the problem of rough configurations completely. Despite the fact that it removed those dislocations discussed in [6, 7] that have been shown to cause the topological susceptibility, χ_t , to diverge in the continuum limit, the presence of other dislocations leaves the fate of the continuum limit of χ_t an open question. The important point is that lattice artifacts can exist at *other* scales independently of the small size artifacts, like the occurrence of negative plaquettes (at least, in nonabelian theories). Presumably, further modifications of the gauge action are necessary to control all dislocations.

The work of JF and UMH was supported in part by the DOE under grants # DE-FG05-85ER250000 and # DE-FG05-92ER40742, and the work of VKM was supported by the Deutsche Forschungsgemeinschaft under research grant Mu 932/1-2. The computations have been carried on the cluster of Alpha workstations at SCRI and on the Convex at Humboldt–Universität zu Berlin. The simulations to determine the $N_\tau = 8$ critical coupling were done on the CM-2 at SCRI.

10 Appendix

It has been observed that the bare lattice coupling is a “bad” coupling constant to investigate asymptotic scaling. Most alternative couplings are extracted from the measured average plaquette values, which we list in Table 10.

Parisi was the first to suggest the use of an effective coupling, β_{eff} , instead of the bare

coupling β [41]. In our analysis we used the effective coupling β_E , obtained from the plaquette by [23]

$$1/\beta_E = \frac{4}{3} \langle 1 - \text{Tr}U_p/2 \rangle \quad . \quad (9)$$

More recently, for a systematic method of improving the lattice perturbation theory, Lepage and Mackenzie advocated to extract a coupling g_V^2 — for SU(2) we have the relation $\beta_X = 4/g_X^2$ for a scheme X — to be interpreted as a running coupling at a scale $3.41/a$, from [42]

$$-\log \langle \text{Tr}U_p/2 \rangle = \frac{3}{16} g_V^2 (1 - 0.0629 g_V^2). \quad (10)$$

The two different couplings are tabulated in Table 11. In perturbation theory the two different schemes are related by

$$\beta_E = \beta_V + 0.6264 + \mathcal{O}(1/\beta_V). \quad (11)$$

We see that the actual values are not too far off from this relation and certainly compatible with the $\mathcal{O}(1/\beta_V)$ correction. It is interesting to note that under the same physical conditions, the deconfinement transition for given N_τ , the improved couplings of the PPM are quite close to their counterparts with SWA.

References

- [1] G.'t Hooft, in *High Energy Physics*, Proceedings of EPS International Conference, Palermo, 1975, Italy, edited by A. Zichichi, (Editrice Compositori, Bologna, 1976); S. Mandelstam, Phys. Rep. **23C** (1976) 245.
- [2] G. Mack, Phys. Rev. Lett. **45** (1980) 1378.
- [3] G. Mack and V. Petkova, Ann. Phys. **123** (1979) 447; Ann. Phys. **125** (1980) 117.
- [4] S. Caracciolo, R.G. Edwards, A. Pelissetto and A.D. Sokal, Phys. Rev. Lett. **71** (1993) 3906.
- [5] V.G. Bornyakov, M. Creutz and V. Mitrjushkin, Phys. Rev. **D44** (1991) 3918.
- [6] D.J.R. Pugh and M. Teper, Phys. Lett. **218B** (1989) 326; Phys. Lett. **224B** (1989) 159.

- [7] M. Göckeler, A.S. Kronfeld, M.L. Laursen, G. Schierholz and U.-J. Wiese, Phys. Lett. **233B** (1989) 192.
- [8] J. Fingberg, U.M. Heller and F. Karsch, Nucl. Phys. **B392** (1993) 493.
- [9] S.P. Booth *et al.*, Phys. Lett. **B275** (1992) 424.
- [10] G. Mack and E. Pietarinen, Nucl. Phys. **B205** [FS5] (1982) 141.
- [11] A. Ambjorn and G. Thorleifsson, NBI preprint NBI-HE-94-30, March 1994.
- [12] G. Bhanot and M. Creutz, Phys. Rev. **D24** (1981) 3212.
- [13] M. Creutz, Phys. Rev. **D21** (1980) 2308.
- [14] A.D. Kennedy and B.J. Pendleton, Phys. Lett. **B156** (1985) 393.
- [15] for a summary see: V. Privman in *Finite Size Scaling and Numerical Simulation of Statistical Systems*, Editor V. Privman, World Scientific 1990, page 1.
- [16] K. Binder, Z. Phys. **B43** (1981) 119; Phys. Rev. Lett. **47** (1981) 693.
- [17] J. Engels, J. Fingberg and M. Weber, Nucl. Phys. **B332** (1990) 737.
- [18] J. Engels, J. Fingberg and D.E. Miller, Nucl. Phys. **B387** (1992) 501.
- [19] J. Engels, J. Fingberg and V.K. Mitrjushkin, Phys. Lett. **B298** (1993) 154.
- [20] A.M. Ferrenberg and D.P. Landau, Phys. Rev. **B44** (1991) 5081.
- [21] M. Albanese *et al.* (Ape Collaboration), Phys. Lett. **B192** (1987) 163.
- [22] C. Michael, Phys. Lett. **B283** (1992) 103.
- [23] F. Karsch and R. Petronzio, Phys. Lett. **139B** (1984) 403.
- [24] M. Teper, Phys. Lett. **B183** (1987) 345.
- [25] C. Michael and M. Teper, Nucl. Phys. **B305** [FS23] (1988) 453.
- [26] M. Lüscher and U. Wolff, Nucl Phys. **B339** (1990) 222.

- [27] Ph. DeForcrand, G. Schierholz, H. Schneider and M. Teper, Phys. Lett. **160B** (1985) 137; M. Lüscher, K. Symanzik and P. Weisz, Nucl. Phys. **B173** (1980) 365.
- [28] R.H. Swendsen, Phys. Rev. Lett. **47** (1981) 1775.
- [29] A. Hasenfratz, P. Hasenfratz, U. Heller and F. Karsch, Phys. Lett. **143B** (1984) 193.
- [30] K.C. Bowler *et al.*, Nucl. Phys. **B257** (1985) 155.
- [31] G. Parisi, R. Petronzio and F. Rapuano, Phys. Lett. **128B** (1983) 418.
- [32] U. Heller and F. Karsch, Nucl. Phys. **B251** [FS13] (1985) 254.
- [33] G. Cella, G. Curci, R. Tripiccionc and A. Vicerè, Phys. Rev. **D49** (1994) 511.
- [34] T. Moretto and M. Teper, bulletin board hep-lat/9312035, Dec. 1993.
- [35] A. Philipps and D. Stone, Commun. Math. Phys. **103** (1986) 599.
- [36] A.S. Kronfeld, M.L. Laursen, G. Schierholz, C. Schleiermacher and U.-J. Wiese, Comp. Phys. Comm. **54** (1989) 109.
- [37] M. Teper, Phys. Lett. **162B** (1985) 357; **171B** (1986) 81, 86.
- [38] C. Michael and M. Teper, Phys. Lett. **199B** (1987) 95.
- [39] C. Michael and J. Perantonis, J. Phys. G18 (1992) 1725.
- [40] S.P. Booth *et al.*, Nucl. Phys. B394 (1993) 509.
- [41] G. Parisi, in *Proceedings of the XXth Conference on High Energy Physics*, Madison 1980.
- [42] G.P. Lepage and P. Mackenzie, Phys. Rev. **D48** (1993) 2250.

N_σ	N_τ	β	meas.	$\langle L \rangle$	$\langle L^2 \rangle$	g_4
8	2	0.080	40000	0.1695(29)	$0.3675(88) 10^{-1}$	-1.290(34)
		0.100	40000	0.1868(25)	$0.4300(90) 10^{-1}$	-1.418(18)
		0.120	40000	0.2044(35)	$0.4985(131) 10^{-1}$	-1.513(24)
12	2	0.080	40000	0.1326(32)	$0.2252(83) 10^{-1}$	-1.257(45)
		0.100	40000	0.1536(42)	$0.2921(113) 10^{-1}$	-1.394(47)
		0.120	40000	0.1843(36)	$0.3904(119) 10^{-1}$	-1.621(25)
8	4	1.250	20000	0.0991(16)	$1.3317(330) 10^{-2}$	-1.022(34)
		1.300	80000	0.1200(10)	$1.8602(246) 10^{-2}$	-1.233(16)
		1.325	80000	0.1315(12)	$2.1686(284) 10^{-2}$	-1.339(17)
		1.350	60000	0.1436(6)	$2.5180(154) 10^{-2}$	-1.434(7)
		1.400	20000	0.1675(13)	$3.2667(392) 10^{-2}$	-1.583(12)
		1.450	20000	0.1915(11)	$4.0151(458) 10^{-2}$	-1.734(11)
12	4	1.250	20000	0.0608(16)	$0.5411(232) 10^{-2}$	-0.669(48)
		1.300	60000	0.0855(13)	$0.9782(221) 10^{-2}$	-1.094(30)
		1.325	60000	0.1017(19)	$1.3126(364) 10^{-2}$	-1.300(36)
		1.350	50000	0.1229(13)	$1.8061(283) 10^{-2}$	-1.509(16)
16	4	1.320	40000	0.0793(20)	$0.8322(314) 10^{-2}$	-1.170(51)
		1.330	40000	0.0905(19)	$1.0258(339) 10^{-2}$	-1.351(31)
		1.350	40000	0.1111(25)	$1.4542(505) 10^{-2}$	-1.556(28)
16	8	1.880	70000	0.0441(3)	$0.2477(25) 10^{-2}$	-1.277(10)
		1.885	87500	0.0457(2)	$0.2622(19) 10^{-2}$	-1.329(9)
		1.890	70000	0.0463(3)	$0.2677(27) 10^{-2}$	-1.344(10)
		1.895	88000	0.0472(3)	$0.2781(32) 10^{-2}$	-1.348(13)
		1.900	70000	0.0481(4)	$0.2869(35) 10^{-2}$	-1.367(13)
		1.905	70000	0.0499(4)	$0.3057(33) 10^{-2}$	-1.411(14)
		1.910	70000	0.0504(7)	$0.3118(60) 10^{-2}$	-1.411(19)
		1.915	70000	0.0524(6)	$0.3329(58) 10^{-2}$	-1.453(18)
		1.920	20000	0.0528(7)	$0.3396(71) 10^{-2}$	-1.442(22)
		1.925	20000	0.0532(7)	$0.3463(82) 10^{-2}$	-1.431(22)
24	8	1.880	80000	0.0340(6)	$0.1483(44) 10^{-2}$	-1.257(27)
		1.885	80000	0.0353(6)	$0.1585(37) 10^{-2}$	-1.289(32)
		1.890	60000	0.0369(5)	$0.1708(35) 10^{-2}$	-1.350(21)
		1.895	94000	0.0394(6)	$0.1892(46) 10^{-2}$	-1.440(24)
		1.900	60000	0.0404(4)	$0.1984(33) 10^{-2}$	-1.447(14)
		1.905	59000	0.0429(6)	$0.2192(49) 10^{-2}$	-1.514(21)

Table 1: Summary of parameters and results of the runs at finite temperature.

N_τ	β_c	$\Delta\beta$
2	0.100(10)	
4	1.332(4)	1.232(14)
8	1.886(6)	0.554(10)

Table 2: Critical couplings from cumulant crossings.

β	L	T	V_0	σ	e	f	range	χ^2/dof	CL
0.1	8	1	0.125(11)	0.674(5)			2.00 - 4.00	3.704/1	0.025
		1	0.211(5)	0.695(3)			1.41 - 5.66	1.567/2	0.536
		2	0.068(4)	0.692(3)			1.00 - 3.00	3.497/1	0.030
		2	0.224(23)	0.681(16)			1.41 - 5.66	0.855/2	0.789
1.332	12	3	0.601(10)	0.1319(15)	0.275(15)	0.72(7)	1.41 - 8.49	7.721/10	0.751
		3	0.599(11)	0.1321(20)	0.286(13)		2.00 - 6.00	0.872/2	0.783
		3	0.588(7)	0.1343(13)	0.254(7)		1.41 - 8.49	1.599/3	0.784
		4	0.597(6)	0.1317(12)	0.267(6)	0.468(14)	1.41 - 8.49	8.758/10	0.619
		4	0.591(19)	0.1332(36)	0.276(22)		2.00 - 6.00	0.243/2	0.975
		4	0.595(11)	0.1323(23)	0.261(11)		1.41 - 8.49	0.544/3	0.982
		5	0.596(10)	0.1318(23)	0.266(10)	0.471(20)	1.41 - 8.49	5.715/10	0.934
		5	0.630(36)	0.1253(71)	0.321(42)		2.00 - 6.00	0.031/2	0.999
	16	5	0.587(21)	0.1342(46)	0.253(21)		1.41 - 8.49	1.028/3	0.915
		3	0.538(21)	0.1386(21)	0.109(55)	1.57(27)	3.00 - 11.31	15.068/11	0.115
		3	0.600(6)	0.1326(10)	0.287(7)		2.00 - 8.00	3.089/4	0.627
		3	0.581(3)	0.1363(7)	0.248(4)		1.41 - 11.31	3.200/5	0.781
		4	0.587(8)	0.1353(14)	0.259(12)	0.694(60)	2.24 - 11.31	7.626/13	0.953
		4	0.590(10)	0.1347(19)	0.277(12)		2.00 - 8.00	2.039/4	0.850
		4	0.577(6)	0.1372(13)	0.244(6)		1.41 - 11.31	1.019/5	0.996
		5	0.583(5)	0.1361(12)	0.255(5)	0.454(11)	1.41 - 11.31	11.604/15	0.807
1.6	12	5	0.599(19)	0.1333(36)	0.289(22)		2.00 - 8.00	1.585/4	0.923
		5	0.581(12)	0.1367(27)	0.249(12)		1.41 - 11.31	2.855/5	0.839
		3	0.569(2)	0.0751(3)	0.238(2)	0.319(8)	1.41 - 8.49	9.285/10	0.550
	16	4	0.571(2)	0.0747(4)	0.240(3)	0.322(9)	1.41 - 8.49	5.681/10	0.936
		5	0.571(3)	0.0746(6)	0.240(3)	0.318(11)	1.41 - 8.49	4.944/10	0.970
		3	0.571(1)	0.0742(2)	0.240(1)	0.316(6)	1.41 - 11.31	8.662/15	0.968
		4	0.568(2)	0.0748(3)	0.237(2)	0.313(7)	1.41 - 11.31	6.076/15	0.998
1.8	12	5	0.569(2)	0.0746(5)	0.237(3)	0.307(9)	1.41 - 11.31	11.096/15	0.847
		6	0.568(3)	0.0750(7)	0.238(3)	0.315(10)	1.41 - 11.31	4.847/15	0.999
		3	0.555(2)	0.0435(3)	0.232(2)	0.267(9)	1.41 - 8.49	3.105/10	0.998
		4	0.559(2)	0.0423(4)	0.236(3)	0.273(10)	1.41 - 8.49	8.076/10	0.707
		5	0.562(3)	0.0417(5)	0.238(3)	0.277(10)	1.41 - 8.49	7.082/10	0.822

Table 3: Fits to the potential approximants $V_T(R)$.

Table 3 continued

β	L	T	V_0	σ	e	f	range	χ^2/dof	CL
1.886	12	3	0.547(2)	0.0334(3)	0.229(2)	0.250(9)	1.41 - 8.49	5.761/10	0.932
		4	0.564(4)	0.0307(6)	0.255(7)	0.212(17)	2.00 - 8.49	1.585/9	0.999
		5	0.574(5)	0.0290(7)	0.268(8)	0.203(19)	2.00 - 8.49	5.110/9	0.924
	16	3	0.540(1)	0.0395(1)	0.223(1)	0.246(4)	1.41 - 11.31	6.390/15	0.997
		4	0.547(2)	0.0347(2)	0.234(3)	0.228(9)	2.00 - 11.31	4.601/14	0.999
		5	0.552(2)	0.0339(3)	0.241(4)	0.225(10)	2.00 - 11.31	1.661/14	1.000
		6	0.546(2)	0.0348(2)	0.227(1)	0.252(6)	1.41 - 11.31	10.413/15	0.893
	7	0.554(3)	0.0336(4)	0.244(5)	0.217(13)	2.00 - 11.31	6.270/14	0.995	
2.0	12	3	0.544(3)	0.0215(5)	0.240(6)	0.202(14)	2.00 - 8.49	1.947/9	0.999
		4	0.555(4)	0.0193(5)	0.255(6)	0.194(16)	2.00 - 8.49	4.759/9	0.947
		5	0.565(8)	0.0171(10)	0.267(14)	0.187(34)	2.00 - 8.49	6.979/9	0.732
2.05	12	3	0.543(3)	0.0165(4)	0.243(5)	0.188(13)	2.00 - 8.49	3.524/9	0.990
		4	0.554(3)	0.0142(4)	0.258(5)	0.178(14)	2.00 - 8.49	4.745/9	0.947
		5	0.567(4)	0.0117(5)	0.275(6)	0.238(50)	2.24 - 8.49	7.526/8	0.521
	16	4	0.541(2)	0.0188(2)	0.245(3)	0.235(26)	2.24 - 11.31	8.927/13	0.881
		5	0.543(2)	0.0181(2)	0.247(3)	0.225(29)	2.24 - 11.31	8.558/13	0.906
		6	0.545(2)	0.0177(3)	0.250(4)	0.241(32)	2.24 - 9.90	9.298/12	0.773
		7	0.559(4)	0.0161(4)	0.278(8)	0.231(34)	2.83 - 11.31	4.970/12	0.995
2.2	12	3	0.513(2)	0.0105(3)	0.228(4)	0.170(10)	2.00 - 8.49	4.649/9	0.952
		4	0.524(4)	0.0083(5)	0.242(6)	0.219(50)	2.24 - 8.49	5.601/8	0.797
		5	0.543(9)	0.0054(10)	0.274(18)	0.223(77)	2.83 - 8.49	3.378/7	0.944
	16	4	0.509(2)	0.0125(3)	0.226(3)	0.204(33)	2.24 - 11.31	7.660/13	0.951
		5	0.514(2)	0.0115(3)	0.232(5)	0.212(51)	2.24 - 11.31	8.938/13	0.880
		6	0.525(5)	0.0100(5)	0.253(11)	0.217(51)	2.83 - 11.31	3.751/12	0.999
	7	0.531(6)	0.0091(6)	0.262(12)	0.234(58)	2.83 - 11.31	9.678/12	0.733	

β	L	t	$m(0^{++})$	$m(2^{++})$ I	$m(2^{++})$ II	$\sigma_{Pol}(L)$
1.332	12	1	1.65(3)	2.42(6)	2.14(7)	0.139(3)
		2	1.26(11)	2.40(77)	2.27(51)	0.156(20)
	16	1	1.59(2)	2.21(6)	2.11(4)	0.144(3)
		2	1.38(11)	2.72(66)	2.21(41)	0.166(48)
1.6	12	1	1.19(3)	1.56(3)	1.60(6)	0.070(1)
		2	0.87(7)	1.41(18)	1.60(19)	0.073(4)
	16	1	1.17(3)	1.61(4)	1.66(5)	0.073(1)
		2	1.08(6)	1.51(17)	1.58(25)	0.071(6)
1.8	12	1	0.89(2)	1.25(2)	1.31(3)	0.0345(12)
		2	0.75(3)	1.13(9)	1.13(10)	0.0319(22)
		3	0.69(7)	1.35(40)	0.89(17)	0.0274(19)
1.886	12	1	0.76(1)	1.14(2)	1.12(2)	0.0244(9)
		2	0.65(3)	1.11(8)	0.96(7)	0.0220(11)
		3	0.57(6)	0.96(16)	1.22(19)	0.0198(12)
	16	1	0.83(1)	1.17(3)	1.14(3)	0.0318(6)
		2	0.70(3)	1.01(6)	1.15(8)	0.0321(12)
		3	0.69(6)	1.15(24)	2.00(57)	0.0323(16)
2.0	12	1	0.73(2)	1.04(2)	0.99(2)	0.0158(9)
		2	0.58(3)	0.83(6)	0.87(6)	0.0136(9)
		3	0.56(5)	0.64(9)	0.84(12)	0.0111(9)
		4	0.45(7)	0.83(29)	0.61(24)	0.0081(7)
2.05	12	1	0.69(2)	0.92(2)	0.93(2)	0.0130(7)
		2	0.56(3)	0.78(5)	0.79(5)	0.0106(8)
		3	0.48(4)	0.63(9)	0.77(9)	0.0083(8)
		4	0.35(5)	0.41(15)	0.78(19)	0.0066(7)
	16	1	0.61(2)	0.84(2)	0.82(1)	0.0149(5)
		2	0.51(2)	0.76(4)	0.78(4)	0.0132(5)
		3	0.44(3)	0.72(9)	0.68(8)	0.0128(8)
		4	0.45(5)	0.70(10)	0.44(10)	0.0117(10)

Table 4: Running glueball masses and string tension $\sigma_{Pol}(L)$.

β_l	L	2	2, extr.	3	3, extr.
1.332	8	1.17(4)	1.17(4)		
	12	1.26(6)	1.23(4)		
	16	1.26(5)	1.23(3)	1.30(5)	1.29(6)
1.6	8	0.763(15)	0.765(22)		
	12	0.773(15)	0.778(18)		
	16	0.774(15)	0.779(18)	0.751(14)	0.743(16)
1.8	8	0.617(8)	0.637(10)		
	12	0.606(9)	0.621(14)		
1.886	8	0.660(12)	0.649(13)		
	12	0.585(9)	0.590(14)		
	16	0.593(13)	0.594(14)	0.585(6)	0.571(4)
2.0	8	0.610(10)	0.606(10)		
	12	0.570(9)	0.556(11)		
2.05	8	0.573(9)	0.569(9)		
	12	0.519(5)	0.530(12)		
	16	0.518(6)	0.528(12)	0.495(3)	0.487(3)
2.2	8	0.526(8)	0.527(7)		
	12	0.511(8)	0.507(10)		
	16	0.512(6)	0.510(11)	0.490(4)	0.482(5)
2.4	8	0.475(12)	0.485(4)		
	12	0.457(6)	0.461(7)		
2.6	8	0.418(10)	0.427(3)		
	12	0.408(6)	0.415(5)		
	16	0.411(5)	0.418(6)	0.408(3)	0.406(4)

Table 5: Blocking MCRG results: the columns with label “ n ” contain the results from matching after n and $n - 1$ blocking steps. The columns with label “ n , extr.” contain the results from extrapolating $\Delta\beta$ to an infinite number of blocking steps according to eq. (7).

β_l	L	basic	tree-level	1-loop	R_{max}	δ_{max}	A_{min}	ΔA_{min}
1.332	8	1.37(11)	1.28(6)	1.27(5)	3	0.200	1	none
	12	1.37(17)	1.19(12)	1.21(7)	4	0.200	2	0
		1.42(16)	1.18(16)	1.33(17)	3	0.200	1	none
	16	1.34(9)	1.24(4)	1.22(3)	5	0.150	2	1
		1.40(7)	1.31(6)	1.24(2)	4	0.200	2	0
1.6	8	0.83(9)	0.72(6)	0.74(6)	3	0.050	1	none
	12	0.85(9)	0.79(5)	0.735(16)	4	0.030	2	0
		0.81(10)	0.74(7)	0.76(8)	3	0.020	1	none
	16	0.84(6)	0.78(3)	0.771(26)	5	0.030	2	1
		0.86(9)	0.81(6)	0.775(27)	4	0.050	2	0
1.8	8	0.67(7)	0.60(3)	0.63(4)	3	0.030	1	none
	12	0.70(6)	0.62(3)	0.582(9)	4	0.020	2	0
		0.62(10)	0.56(5)	0.59(6)	3	0.020	1	none
1.886	8	0.63(8)	0.58(3)	0.60(4)	3	0.050	1	none
	12	0.65(5)	0.59(3)	0.552(5)	4	0.020	2	0
		0.60(9)	0.54(4)	0.557(42)	3	0.020	1	none
	16	0.63(5)	0.57(2)	0.561(16)	5	0.015	2	1
		0.66(6)	0.58(3)	0.557(7)	4	0.015	2	0
2.0	8	0.65(9)	0.54(4)	0.55(6)	3	0.050	1	none
	12	0.59(6)	0.56(4)	0.518(7)	4	0.020	2	0
		0.53(10)	0.49(5)	0.52(5)	3	0.020	1	none
2.05	8	0.59(12)	0.49(4)	0.51(6)	3	0.050	1	none
	12	0.58(8)	0.55(4)	0.498(9)	4	0.020	2	0
		0.51(11)	0.47(4)	0.49(6)	3	0.020	1	none
	16	0.55(6)	0.516(24)	0.507(12)	5	0.010	2	1
		0.60(6)	0.533(24)	0.512(8)	4	0.010	2	0

Table 6: Ratio method MCRG results: the two lines for sizes 12 and 16 represent different cuts on the Wilson loops and ratios considered. The various cuts are described in the text.

Table 6 continued

β_l	L	basic	tree-level	1-loop	R_{max}	δ_{max}	A_{min}	ΔA_{min}
2.2	8	0.60(6)	0.46(3)	0.52(5)	3	0.050	1	none
	12	0.59(6)	0.52(5)	0.460(5)	4	0.020	2	0
		0.53(11)	0.43(5)	0.47(5)	3	0.020	1	none
	16	0.53(5)	0.500(19)	0.494(10)	5	0.010	2	1
		0.57(7)	0.516(25)	0.493(5)	4	0.015	2	0
2.4	8	0.56(12)	0.47(3)	0.48(5)	3	0.050	1	none
	12	0.57(7)	0.49(4)	0.433(8)	4	0.020	2	0
		0.49(12)	0.38(6)	0.43(5)	3	0.020	1	none
2.6	8	0.48(11)	0.42(2)	0.44(4)	3	0.050	1	none
	12	0.53(6)	0.44(4)	0.394(6)	4	0.020	2	0
		0.45(12)	0.34(5)	0.40(5)	3	0.020	1	none
	16	0.48(4)	0.428(20)	0.419(9)	5	0.010	2	1
		0.50(4)	0.441(17)	0.422(4)	4	0.010	2	0

N_τ	$T_c/\Lambda_{\overline{\text{MS}}}$	$T_c/\Lambda_{\overline{\text{MS}} _E}$	$\sqrt{\sigma}/\Lambda_{\overline{\text{MS}}}$	$\sqrt{\sigma}/\Lambda_{\overline{\text{MS}} _E}$
2	0.043(1)	0.749(20)	0.07074(40)	1.2363(69)
4	0.198(2)	1.058(11)	0.29172(4)	1.5562(6)
8	0.380(6)	1.102(18)	0.56025(8)	1.6231(1)

Table 7: Asymptotic (2-loop) scaling of T_c , determined from the critical couplings $\beta_c(N_\tau)$, and of the string tension, determined from fits to the potential. Listed are the results with the bare and the effective, (β_E), coupling schemes.

N_τ	β_c	σ	$\sqrt{\sigma}/T_c$
2	0.100(10)	0.6810(16)	1.65(6)
4	1.332(4)	0.1353(14)	1.48(2)
8	1.886(6)	0.0339(3)	1.47(3)

Table 8: Scaling of the ratio of the string tension from fits to the potential and the critical temperature.

β	L	Hot, PS	10c, N1	10c, N2	15c, PS	15c, N1	15c, N2	20c, N1	20c, N2
1.332	8	19.3(1.0)	2.90(13)	5.12(20)	4.41(20)	2.85(13)	4.61(19)	2.79(12)	4.28(18)
	12	17.5(5)	2.90(9)	4.00(11)	4.51(14)	2.89(9)	3.98(11)	2.83(9)	3.88(11)
	16		2.97(9)	3.58(10)		2.91(9)	3.49(10)	2.81(9)	3.38(10)
1.6	8	5.47(19)	1.28(5)	2.11(7)	1.82(7)	1.24(5)	1.88(7)	1.19(5)	1.74(7)
	12	5.44(17)	1.36(4)	2.08(6)	1.92(6)	1.35(4)	1.98(6)	1.32(4)	1.87(5)
	16		1.37(6)	1.78(7)		1.39(6)	1.80(7)	1.37(6)	1.78(7)
1.8	8	1.55(7)	0.24(2)	0.39(2)	0.33(2)	0.22(1)	0.35(2)	0.20(1)	0.31(2)
	12	1.20(8)	0.60(3)	0.91(4)	0.80(4)	0.61(3)	0.85(4)	0.61(3)	0.83(4)
1.886	8	0.84(6)	0.115(16)	0.190(25)	0.164(23)	0.107(16)	0.168(23)	0.098(15)	0.159(23)
	12	1.28(7)	0.320(20)	0.463(27)	0.408(26)	0.323(21)	0.437(27)	0.323(21)	0.423(27)
	16		0.377(17)	0.542(22)		0.380(17)	0.517(22)	0.318(17)	0.505(21)
2.0	8	0.41(3)	0.031(5)	0.051(8)	0.047(7)	0.028(5)	0.047(7)	0.025(4)	0.039(7)
	12	0.54(3)	0.141(13)	0.200(19)	0.183(17)	0.144(14)	0.194(19)	0.144(14)	0.189(19)
2.05	8	0.29(3)	0.022(9)	0.037(13)	0.032(12)	0.020(9)	0.032(12)	0.017(8)	0.027(12)
	12	0.40(3)	0.094(11)	0.130(16)	0.121(15)	0.094(11)	0.124(16)	0.092(11)	0.116(14)
	16		0.157(12)	0.215(16)		0.159(12)	0.205(16)	0.160(12)	0.202(15)
2.2	12	0.133(10)	0.013(4)	0.018(5)	0.015(4)	0.012(4)	0.016(4)	0.012(4)	0.015(4)
	16		0.051(7)	0.065(8)		0.052(7)	0.063(8)	0.051(7)	0.061(7)

Table 9: Topological susceptibility $\times 10^4$ and cooling. “PS” denotes the Phillips–Stone charge, “N1” the naive (non–integer) charge and “N2” the naive charge but rounded away from zero.

β	$L = 8$	$L = 12$	$L = 16$
0.1	0.54706(4)		
1.332	0.41695(7)	0.41685(2)	0.41685(1)
1.6	0.38753(7)	0.38756(2)	0.38755(2)
1.8	0.36651(7)	0.36666(3)	
1.886	0.35773(7)	0.35785(3)	0.35792(2)
2.0	0.34651(6)	0.34656(3)	
2.05	0.34161(6)	0.34173(3)	0.34173(2)
2.2	0.32746(6)	0.32740(3)	0.32747(2)
2.4	0.30912(4)	0.30913(3)	
2.6	0.29182(4)	0.29182(3)	0.29181(1)

Table 10: Average plaquette values, $\langle 1 - \text{Tr}U_p/2 \rangle$.

β	β_E	g_E^2	β_V	g_V^2
0.100	1.37096	2.91765		
1.332	1.79921	2.22320	1.06091	3.77036
1.600	1.93518	2.06699	1.21222	3.29973
1.800	2.04549	1.95552	1.33190	3.00323
1.886	2.09585	1.90853	1.38590	2.88621
2.000	2.16413	1.84832	1.45862	2.74232
2.050	2.19472	1.82256	1.49103	2.68270
2.200	2.29078	1.74613	1.59229	2.51211
2.400	2.42616	1.64869	1.73384	2.30701
2.600	2.57008	1.55637	1.88320	2.12404

Table 11: Effective couplings from the $L = 12$ plaquette values, except for $\beta = 0.1$ where the $L = 8$ value was used.